

Ultrashort Microwave Pulses Generated Due to Three Magnon Interactions

Valeri T. Synogach, Yuri K. Fetisov,* Christoph Mathieu, and Carl E. Patton

Department of Physics, Colorado State University, Fort Collins, Colorado 80523

(Received 28 February 2000)

Extremely narrow 2 ns wide microwave pulses are generated from nonlinear magnetostatic surface waves in yttrium iron garnet films. The shortest output pulse with the highest amplitude is achieved for input power levels of about 300 mW and a carrier frequency below 3.3 GHz. The results are explained within the model based on dipole exchange spin wave modes involved in three magnon processes. The characteristic time for these processes to develop, as estimated from the smallest fall time of output pulse, is 1 ns. The relevant modes are verified by Brillouin light scattering.

PACS numbers: 75.30.Ds, 76.50.+g, 85.70.Ge

Nonlinear magnetic excitations at microwave frequencies in yttrium iron garnet (YIG) films have been used extensively for the production of short microwave pulses. In addition to the technical interest in short pulses, the detailed understanding of the nonlinear interactions behind such pulse formation represents important new physics. Because of the low damping and low power thresholds in YIG films, a rich variety of nonlinear effects can be realized. These include parametric instabilities, spin wave solitons, and chaos [1,2].

Up to now, short pulse formation has been achieved mainly through the generation of microwave magnetic envelope (MME) solitons in YIG films [3–5]. Such solitons are formed due to the balance between the dispersion and the nonlinear response of the magnetostatic wave (MSW) excitations and are related to four magnon interactions. The narrowest pulses obtained from MME solitons are in the 5–10 ns width range [3,4]. Here, the input pulses were short and only slightly longer than the final soliton pulse. Long input pulses have also been used to generate short magnetostatic wave leading or trailing edge spikes [6,7]. Even there, however, the output pulses were more than an order of magnitude wider than those presented below.

This Letter reports on the generation of ultrashort microwave pulses through nonlinear three magnon interactions for magnetostatic surface wave (MSSW) excitations. Pulses as narrow as 2 ns can be produced from a long input pulse when the signal frequency is below 3.3 GHz. Three magnon processes are allowed for low wave number MSSW excitations in YIG only for frequencies below this limit [8]. The smallest fall time for these narrow pulses was 1 ns. This is interpreted as the characteristic time for the three magnon process to develop. The narrowing effect is most pronounced at input power levels of about 300 mW, which is at least 30 dB above the threshold power for three magnon processes. The power regime for the ultrashort pulse formation is, therefore, highly nonlinear. The pulses obtained here (i) are the shortest microwave envelope pulses ever produced from long input pulses and (ii) are realized through an entirely new physical process.

The measurements here were done with the same techniques as in [4]. The experiments utilized an MSW antenna

structure with a 10.2 μm thick, 16 mm long, and 2 mm wide YIG film. The YIG strip was magnetized in plane by a static magnetic field perpendicular to the strip and the MSSW propagation direction. The structure consisted of one fixed and one movable 50 μm wide microstrip antenna placed perpendicular to the YIG strip. The input microwave signals were obtained with a cw synthesizer, a fast microwave switch, and a power amplifier. Signals were analyzed with an HP71500A microwave transition analyzer. The pulse duty cycle was kept below 1% to avoid heating effects. All data shown below are for an input pulse width of 100 ns. The overall results, however, were independent of the input pulse width in the range 50 ns–100 μs .

Figure 1 shows the essential aspects of the pulse narrowing. Panels (a) and (b) show the evolution of output power vs time profiles with increasing input power level P_{in} at 1.8 GHz and 4.9 GHz, respectively. The static magnetic field was 150 Oe for (a) and 1 kOe for (b). The antenna spacing was 4.5 mm. Panel (a) shows pulse distortion in the form of a transient decay to zero which occurs at the end of the pulse. The threshold for this effect is typically below 0.2 mW. As the power increases, the decay becomes shorter and finally one obtains a narrow leading edge spike. Spikes with the smallest width of about 2.5 ns and highest peak power are obtained at some optimal P_{in} level around 300 mW. Above this power level, the pulse broadens and drops in amplitude. Panel (b) shows a rather different nonlinear effect. The transient decay now extends over the entire width of the input pulse and never clamps to zero. The decay time does decrease as P_{in} is increased. However, even the smallest decay time at $P_{\text{in}} = 1 \text{ W}$ is much larger than the smallest spike width in panel (a).

The different results for 1.8 and 4.9 GHz are attributed to the onset of three magnon processes below the 3.3 GHz transition point. Figure 2 provides further support for such a transition. Graph (a) shows the full width of the output pulse at a point close to the baseline as a function of frequency. The insets show the actual pulse shapes for frequencies above and below the transition. Graph (b) shows the frequency dependences of the spike peak power, P_{max} , and the corresponding power level at the end of the pulse,

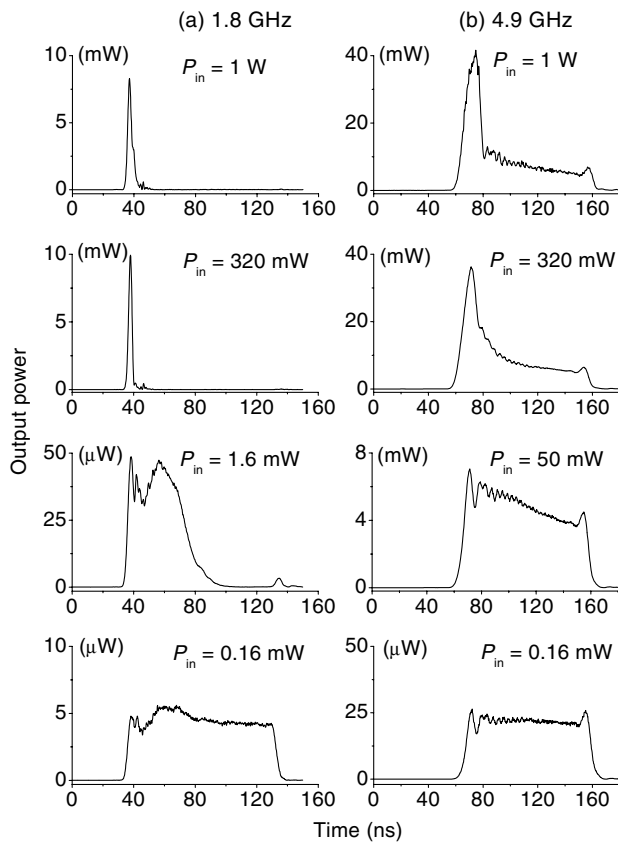


FIG. 1. Output power vs time at 1.8 and 4.9 GHz, and for input peak power P_{in} values as indicated. The antenna spacing and input pulse width were 4.5 mm and 100 ns, respectively. The static magnetic field of 150 Oe for (a) and 1 kOe for (b) was in the film plane and perpendicular to the pulse propagation direction.

P_{end} . The nominal antenna separation was 3 mm. The static field and the input power were adjusted slightly at each frequency to optimize the P_{max} response. Graph (a) shows an extremely sharp transition for the pulse width. Above 3.7 GHz, the width simply matches the input pulse width. Below 3.3 GHz, the original wide pulse is clamped to zero, except for the ultrashort leading edge spike. Graph (b) shows that P_{end} drops abruptly by 30 dB as one moves below 3.3 GHz, while P_{max} remains essentially unchanged.

Figure 3 provides further data on the ultrashort pulse characteristics. Graph (a) shows the power profile for a representative pulse on an expanded time scale. Graph (b) shows the power frequency spectrum of that pulse. Graph (c) shows a cw power frequency transmission loss profile. All data are taken at a static magnetic field of 150 Oe and a 3 mm antenna separation. The input power was 300 mW for graphs (a) and (b), and 0.2 mW for (c). The pulse width at half power in (a) is 2.2 ns. The corresponding power frequency spectrum of the pulse is spread over the range of about 1 GHz, as shown in (b). The more important property of the spectrum in (b), however, is the shape. Apart from a small peak at the signal frequency, this shape closely matches the cw transmission loss profile for the

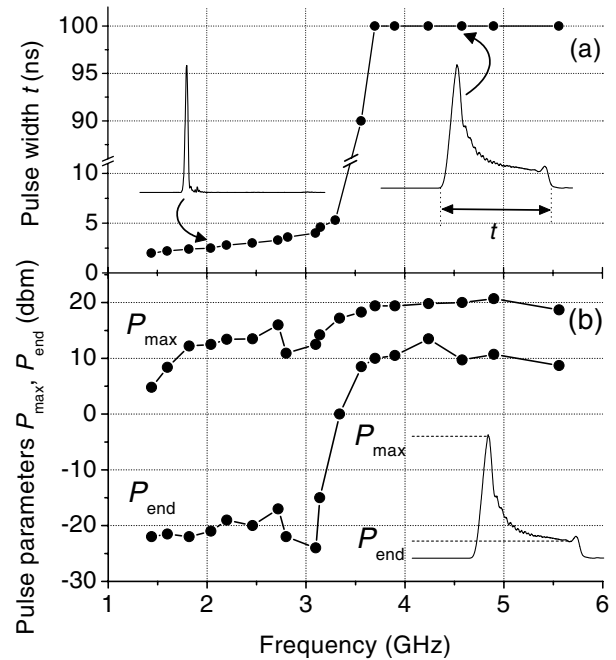


FIG. 2. (a) Output pulse at a point near the baseline vs frequency. The inset shows representative pulse profiles above and below 3.3 GHz. (b) Frequency dependence of the pulse power parameters P_{max} and P_{end} identified in the inset. For each frequency, the static field and input power were adjusted to obtain the highest value of P_{max} . The nominal antenna separation was 3 mm.

MSSW pass band in (c). This means that the excitations which make up the pulse in (a) are spread over the entire MSSW pass band. Although not shown in (b), one finds an additional weak and barely resolvable peak in the pulse spectrum at 0.9 GHz, one-half the signal frequency.

Figure 4 shows additional data on the ultrashort pulses. Pulse peak power, P_{max} , and pulse width at $P_{max}/2$ are shown as a function of propagation time. The propagation time was varied through a change in the antenna separation. The top scale shows the antenna separation, based on calibration points at 3 and 10 mm. The carrier frequency, static magnetic field, and P_{in} level were 1.8 GHz, 150 Oe, and 320 mW, respectively. These data show that P_{max} decreases with antenna separation, but with one pronounced local maximum for a separation of 3 mm. The pulse half-width increases monotonically with antenna separation. At the optimal separation of 3 mm, one obtains a clean, sharp, and narrow output pulse. For smaller separations, there are additional small amplitude peaks around the main peak. For larger separations, the pulse broadens and drops in amplitude.

Lower frequencies tend to produce narrower pulses. However, the pulse shape is relatively insensitive to changes in the frequency as long as one is below 3.3 GHz. This means that the formation process is not a sensitive function of the MSSW carrier wave number. For YIG films in the 5–15 μm thickness range, thicker films tend to produce shorter and cleaner pulses.

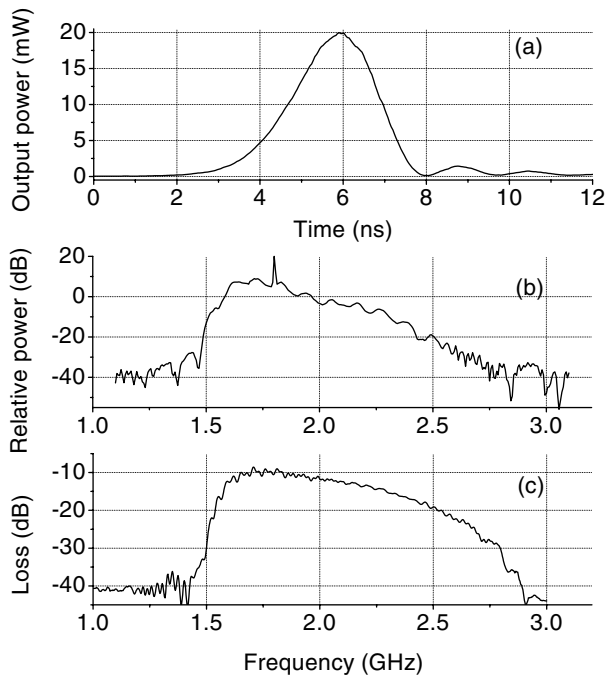


FIG. 3. (a) Power vs time profile for a typical ultrashort pulse. The pulse was formed from a 100 ns wide, 300 mW high input pulse at 1.8 GHz. The magnetic field and antenna separation were 150 Oe and 3 mm, respectively. (b) Corresponding power frequency spectrum for the pulse in (a). (c) cw transmission loss vs frequency profile for the same field and a low input power of 0.2 mW.

The ultrashort pulse formation can be explained by a two step three magnon process. First, the low wave number MSSW signal at frequency f_s generates parametric

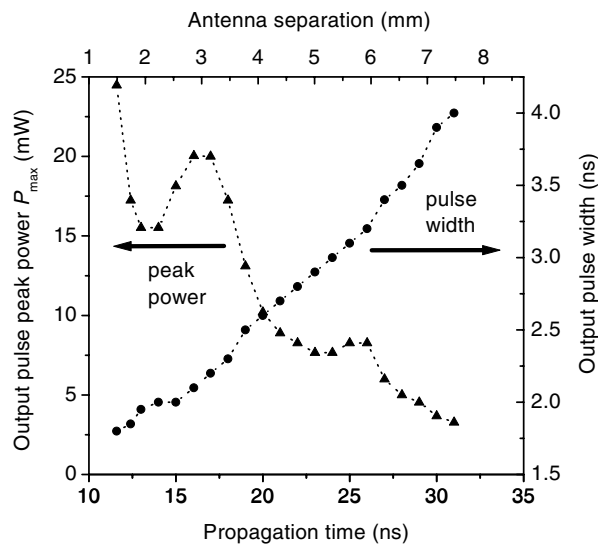


FIG. 4. Pulse peak power P_{max} and pulse width at $P_{max}/2$, as indicated, as a function of the pulse propagation time from input to output. The antenna separation is shown on the top scale. The input pulse width was 100 ns, the input peak power was 320 mW, the frequency was 1.8 GHz, and the static magnetic field was 150 Oe.

magnons at frequencies near $f_s/2$ through three magnon splitting. The allowed modes for these parametric magnons are associated with the available dipole exchange spin wave (DESW) branches close to $f_s/2$. These modes are spread over a wide range of wave numbers and frequencies. Second, at high power, these parametric DESW magnons produce a new band of MSSW excitations through three magnon confluence. This new band of excitations is centered at f_s and has a spread spectrum which extends over the entire MSSW pass band. This spectrum in the time domain corresponds to the ultrashort pulse found experimentally.

Consider first the modes involved in the three magnon process. The initial MSSW magnon at frequency f_s and wave vector \mathbf{k}_s splits into two parametric magnons with frequencies $f_{1,2}$ and wave vectors $\mathbf{k}_{1,2}$. In order to satisfy momentum conservation, the $\mathbf{k}_{1,2}$ vectors must be nearly parallel to the magnetic field and oppositely directed. The allowed $f_{1,2}$ and $\mathbf{k}_{1,2}$ values are determined by the dispersion relation for the DESW modes in the film.

Figure 5 shows dispersion diagrams of frequency f vs wave number k which demonstrate the splitting and mode selection process. The MSSW dispersion curve in Fig. 5(a) was obtained from Damon-Eshbach theory [9]. The DESW curves in (a) and (b) were calculated from [10]. All curves were computed for a magnetic field, frequency,

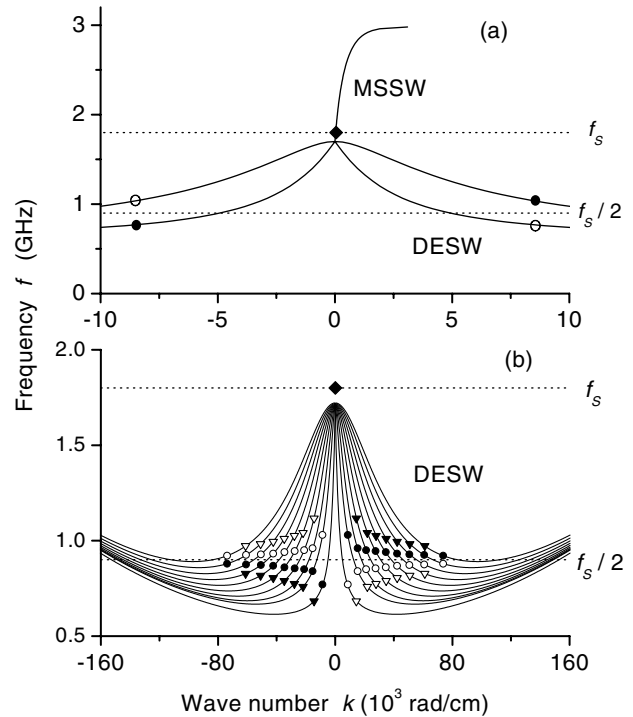


FIG. 5. Calculated dispersion diagrams of frequency f vs wave number k for the magnetostatic surface wave (MSSW) branch and various dipole exchange spin wave (DESW) branches. The solid diamond indicates the MSSW operating point frequency at $f = f_s = 1.8$ GHz. The solid and open circles and triangles indicate DESW modes with opposite k values and frequencies equally shifted above and below $f_s/2$.

and film thickness of 150 Oe, 1.8 GHz, and 10.2 μm , respectively, the same as for the data in Fig. 3.

Graph (a) shows the MSSW dispersion branch for wave vectors perpendicular to the magnetic field and the two lowest DESW branches for wave vectors parallel to the field. The solid diamond shows the MSSW operating point at $f = f_s = 1.8$ GHz and $k = k_s = 150$ rad/cm. The pairs of modes which satisfy energy and momentum conservation under three magnon splitting are indicated by solid and open circles, respectively. For a given pair, one mode is above and one is below the $f_s/2$ reference line by the same amount δf and the k values have opposite sign.

Graph (b) has the same format as (a), but with a compressed k scale. Graph (b) shows the first ten DESW branches which extend below the $f_s/2$ line. The pairs of modes which satisfy energy and momentum conservation are shown by solid and open circles and triangles. The circles indicate pairs of such modes on adjacent DESW branches. The triangles correspond to nonadjacent branches with two branches in between. There are more such pairs of modes for other branches.

Figure 5(b) shows that the frequency separation δf for different pairs of DESW magnons can take on a range of values. It is this spread in frequencies which leads to the ultrashort pulse formation. The maximum value of the frequency separation, δf_{max} , is 220 MHz. This corresponds to the first pair of triangle points in Fig. 5(b) at $k \approx \pm 14 \times 10^3$ rad/cm. Through the confluence process, the various DESW magnons coalesce to produce secondary MSSW magnons with frequencies shifted from f_s by as much as $2\delta f_{\text{max}}$. The full bandwidth of these MSSW magnons is $4\delta f_{\text{max}}$, or 880 MHz. This corresponds to a pulse width of about 2.3 ns in the time domain. This width closely matches the experimental 2.2 ns pulse width in Fig. 3. The pulse fall time of 1 ns, from graph (a) of Fig. 3, can be interpreted as the characteristic time for the three magnon process to develop.

The above model is supported by direct measurements of nominal half frequency magnons at the wave vectors close to those indicated in Fig. 5(b). These data were obtained by wave vector selective Brillouin light scattering (BLS) techniques [11]. A full description of these BLS results will be published separately. The mechanism is also consistent with previous microwave and BLS results [8,12–15] on three magnon processes from cw MSSW high power experiments.

The response above 3.3 GHz, as in Fig. 1(b), is defined by a different physical process, namely, the four magnon

parametric instability. The threshold for this process is higher and the nonlinear pulse narrowing for similar power levels is much less effective. The smallest value of the pulse decay time observed in this case may be interpreted as the characteristic time for four magnon processes to develop. The estimated value of this time is about 5 ns, which is much longer than the 1 ns characteristic time estimate for three magnon processes.

This work was supported in part by the National Science Foundation, Grant No. DMR-9801649 and the U.S. Army Research Office, Grant No. DAAG55-98-1-0430. The authors acknowledge Dr. B. A. Kalinikos for helpful discussions and Mr. R. G. Cox for help with the automation of the experiments.

*Permanent address: Physics Department, Moscow Institute of Radioengineering, Electronics and Automation, Prospect Vernadskogo 78, Moscow 117454, Russia.

- [1] A. K. Zvezdin and A. F. Popkov, Zh. Eksp. Fiz. **84**, 606 (1983) [Sov. Phys. JETP **57**, 350 (1983)].
- [2] *Nonlinear Phenomena and Chaos in Magnetic Materials*, edited by P. E. Wigen (World Scientific, Singapore, 1994).
- [3] B. A. Kalinikos, N. G. Kovshikov, and A. N. Slavin, IEEE Trans. Magn. **26**, 1477 (1990).
- [4] N. G. Kovshikov, B. A. Kalinikos, C. E. Patton, E. S. Wright, and J. M. Nash, Phys. Rev. B **54**, 15 210 (1996).
- [5] B. A. Kalinikos, N. G. Kovshikov, and C. E. Patton, Phys. Rev. Lett. **80**, 4301 (1998).
- [6] N. G. Kovshikov, P. A. Kolodin, and A. N. Slavin, Pis'ma Zh. Tekh. Fiz. **15**, 37 (1989) [Sov. Tech. Phys. Lett. **15**, 15 (1989)].
- [7] D. J. Mar, L. M. Pecora, F. J. Ratchford, and T. L. Carrol, Chaos **7**, 803 (1997).
- [8] A. M. Mednikov, Fiz. Tverd. Tela (Leningrad) **23**, 242 (1981) [Sov. Phys. Solid State **23**, 136 (1981)].
- [9] R. W. Damon and J. R. Eshbach, J. Phys. Chem. Solids **19**, 308 (1961).
- [10] B. A. Kalinikos, Sov. Phys. J. **24**, 718 (1981).
- [11] H. Xia, P. Kabos, H. Y. Zhang, P. A. Kolodin, and C. E. Patton, Phys. Rev. Lett. **81**, 449 (1998).
- [12] G. Srinivasan and C. E. Patton, Appl. Phys. Lett. **47**, 759 (1985).
- [13] A. G. Temiryazev, Sov. Phys. Solid State **29**, 179 (1987).
- [14] G. A. Melkov and S. V. Sholom, Zh. Eksp. Teor. Fiz. **96**, 712 (1989) [Sov. Phys. JETP **69**, 403 (1989)].
- [15] M. Sparks, *Ferromagnetic Relaxation Theory* (McGraw-Hill, New York, 1964).